ACS APPLIED ENERGY MATERIALS

www.acsaem.org Article

Tailoring the Structure–Property Relationships of Innovative Flowerlike TiO_2 Structures in a Fiber-Shaped Dye-Sensitized Solar Cell

Chen Lin, Brishty Deb Choudhury,[†] Rigobert Ybarra,[†] Sk Md Ali Zaker Shawon, Haimanti Majumder, Javier Soliz-Martinez, Nicolas Dimakis, Karen Lozano, and Mohammed Jasim Uddin*

Cite This: *ACS Appl. Energy Mater.* 2024, 7, 2329–2337 Read Online

ACCESS | Metrics & More | Article Recommendations | Supporting Information

ABSTRACT: In dye-sensitized solar cells, one-dimensional (1D) Titanium dioxide (TiO_2) nanostructures like nanotubes, nanorods, and nanowires (NWs) are very commonly used as photoanode materials for dye molecule absorption due to their unique properties to enhance the cell performance. However, 1D TiO_2 nanostructures have relatively low surface areas because of the free space between them. Herein, this paper reports an alkali hydrothermal method to prepare different TiO_2 structures on Ti wire without using any surfactants. The morphology of the samples has been studied with the reaction time and analyzed by scanning electron microscopy. The study reveals that this common strategy could form not only 1D NWs but also different types of flowerlike TiO_2 hierarchical structures. Different structures could be achieved by carefully adjusting the reaction parameters of the hydrothermal reaction. These structures were used as photoanodes to assemble fiber-shaped dye-sensitized solar cells, and the photoinduced photocurrent density–voltage curves were measured for these devices.

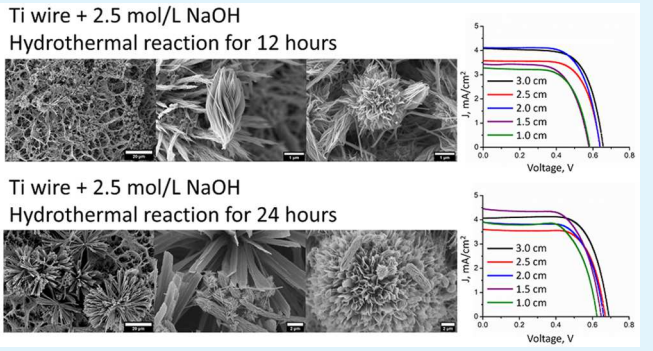

KEYWORDS: *TiO_2, flowerlike, photovoltaic, dye-sensitized solar cells, flexible cells*

INTRODUCTION

Titanium dioxide (TiO_2) is a widely used material in many different commercial areas such as paints, toothpaste, sunscreens, etc.,[1−6] because it is stable, biologically and environmentally benign, inexpensive, and abundant in nature. Moreover, excellent optical and electrical properties endowed TiO_2 with extremely promising potential in photovoltaic applications.[7−12] Compared to other metal oxides, solar cells based on TiO_2 electrodes show the highest stability in performance and largest energy conversion efficiency.[9,13−16]

However, TiO_2 possesses two large disadvantages for applications in solar energy conversion: relatively poor charge-transport property and wide band gap. In fact, these two limitations can be overcome via engineering materials to form nanostructures. It is well-known that quantum confinement effects in nanomaterials can alter the transport behaviors of charge carriers and shift the electronic band structure.[17] For example, in dye-sensitized solar cells (DSSCs), the key component is a photoanode typically consisting of mesoporous TiO_2 with dye molecules adsorbed on it. It is believed that percolation in the TiO_2 nanoparticle network in traditional photoanodes causes a loss of electrons, thus limiting the device performance.[18−21] This major drawback can be solved by using highly ordered one-dimensional (1D) TiO_2 nanostructures, such as nanowires (NWs) and nanotubes (NTs), in photoanodes because these structures can provide direct conducting pathways and reduce charge-carrier recombination.[22−24] Therefore, it is crucial to control the nanostructures of TiO_2 to achieve the appropriate size, morphology, crystalline phases, and specific surface area for diverse applications because these parameters determine the properties of TiO_2 nanomaterials.[1,25−29]

Among all of the TiO_2 nanomaterials, 1D nanostructures have unique properties, for example, confined electron/photon transport and good mechanical properties, and hence are widely used not only in solar cells but also in other applications such as batteries and photoelectrochemical cells for effective charge separation and collection.[19,30,31] Despite these advantages, 1D TiO_2 nanomaterials have relatively low surface areas because of the free space between the individual nanostructures. Thus, researchers have worked to develop hierarchical

Received: December 11, 2023
Revised: February 23, 2024
Accepted: February 26, 2024
Published: March 6, 2024

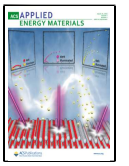

https://doi.org/10.1021/acsaem.3c03091
ACS Appl. Energy Mater. 2024, 7, 2329−2337

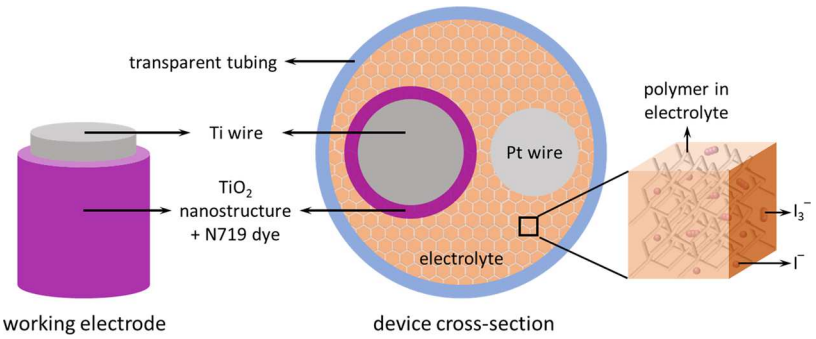

Figure 1. Schemes of the WE and cross-sectional devices.

TiO_2 nanostructures to solve this issue, such as flowerlike TiO_2 structures. The microflower morphology provides multiple advantages of light scattering, increased dye loading, and a direct transport pathway. For example, Wang et al. reported the synthesis of TiO_2 flowerlike nanostructures by a Ti−H_2O_2 oxidation−hydrothermal method.[32] Hyam et al. fabricated rutile TiO_2 nanoneedle flowers through electrochemical anodization in a perchloric acid solution under room temperature.[33] In Xiang et al.'s work, hierarchically flowerlike TiO_2 superstructures with exposed {001} facets were obtained through a solvothermal strategy using titanate NTs as precursors.[34] Shao et al. adopted a hydrothermal method to treat a Ti plate with a sodium hydroxide (NaOH) solution and obtained TiO_2 microflowers formed by TiO_2 nanobelts.[35] Xu et al. showed the preparation of flowerlike TiO_2 particles using a template-free solvothermal approach by using tetrabutyl tinanate (TBT).[36] Zhao et al. obtained 3D flowerlike TiO_2 hierarchical microstructures by a hydrothermal method using TBT and poly(ethylenepyrrole) in an acetic acid solution.[37] Li et al. also reported flowerlike TiO_2 nanostructures dominant with {001} facets that were similar to those in Xiang et al.'s work,[34] while they adopted a one-pot, template-free solvothermal method using TBT as the Ti source without any precursors.[38] In Que et al.'s paper, flowerlike structures with highly crystallized anatase TiO_2 nanosheets were synthesized through a one-pot hydrothermal process, using poly(vinylpyrrolidone), titanium isopropoxide (TTIP), and hydrogen fluoride.[39] Zong et al. reported 3D flowerlike morphology of TiO_2 obtained by a hydrothermal method with TTIP and acetic acid.[40] Liu et al. demonstrated a direct synthesis of flowerlike TiO_2 crystals using TBT and ethylene glycol.[41]

In the above-described studies, some mainly focus on the photocatalytic properties of these unique hierarchical structures.[32,34,40,41] In some works,[33,35,37,39] the photovoltaic properties of TiO_2 flowerlike structures were investigated, while all of them utilized a sandwich-shaped flat cell design with conductive glasses. The rigidity of the devices forbids any application where flexibility is required. Besides, TiO_2 hierarchical flowerlike structures obtained in these works were either precipitated out in the reaction solution[33,34,36−41] or directly grown on substrates,[35] no matter whether metallic Ti[33,35] or Ti-containing compounds[34,36−41] were used as Ti source. If photovoltaic properties of these structures need to be investigated, extra steps are required for sample separation and purification, as well as deposition and stabilization of these materials on conductive substrates. These two problems can be easily solved by adopting the design of fiber-shaped dye-sensitized solar cells (FDSSCs) based on TiO_2 nanostructures directly grown on Ti wires. The surface of the Ti wire could be treated to obtain the desired TiO_2 nanostructure, while the inner intact metal could behave as the conductive base for the photoanode. For example, Zhang et al. used an anodization method to obtain Ti NT arrays on Ti wires for FDSSCs;[42] Liu et al. synthesized TiO_2 NW arrays on Ti wires via a NaOH solution hydrothermal reaction;[43] Chu et al. reported seeded growth of treelike TiO_2 nanoarrays on Ti and other metal wires for FDSSCs.[44] However, to our best knowledge, there is no report about the direct fabrication of flowerlike TiO_2 structures on Ti wires as the photoanode material for FDSSCs. In this paper, we report the fabrication of novel TiO_2 flowerlike hierarchical structures on top of Ti wires via a hydrothermal method in a NaOH solution. In the scanning electron microscopy (SEM images, different types of flowerlike structures are well observed. Photovoltaic properties are also reported for DSSCs fabricated with flowerlike TiO_2 structures on 1D TiO_2 NW arrays.

EXPERIMENTS

Fabrication of TiO_2 Nanostructures. Eight Ti wires (ϕ = 250 μm and length 4−5 cm) were subsequently cleaned ultrasonically in ethanol and acetone for 15 min to remove any impurities. The treated wires were then put in 20−30 mL of a 2.5 M NaOH aqueous solution in 50 mL Teflon-lined stainless-steel autoclaves. The sealed autoclaves were put in an electric furnace at 220 °C for various times (4, 8, 12, 16, 20, and 24 h) followed by natural cooling to room temperature. Then these Ti wires were washed repeatedly with Milli-Q water several times to remove excess NaOH solution. After that, samples were immersed in a 1 M HCl solution for 1 h to replace Na^+ with H^+. Finally, the as-prepared samples were calcined at 550 °C for 30 min.

Fabrication of FDSSCs. The as-prepared photoanodes were immersed in a 0.5 mM N719 dye solution (a solvent mixture of acetonitrile and *tert*-butyl alcohol in a volume ratio of 1:1) for 72 h. After that, the photoanodes were washed repeatedly with acetonitrile to remove excess dye solution. A Pt wire (ϕ = 125 μm) was aligned parallel to the photoanode in a transparent capillary tube. The electrolyte was injected into this capillary using a pipet. The electrolyte was prepared by dissolving 0.5 M lithium iodide, 0.05 M iodine, and 0.5 M *tert*-butylpyridine and brought up to 10 mL volume in 3-methoxypropionitrile. Poly(vinylidene fluoride-*co*-hexafluoropropylene) (5 wt %) was added to this solution and dissolved overnight with mild heating to make a homogeneous solution.

Morphological and Photovoltaic Characterizations. The morphological characterization was done using SEM (EVO LS10 STEM). The photocurrent−voltage measurements were carried out using a VersaSTAT3 potentiostat (Princeton Applied Research) running cyclic voltammetry with a scan rate of 50 mV/s. A Honle Solar Simulator 400 with an AM 1.5G spectrum (100 mW/cm^2) was used to simulate sunlight for irradiating the cells. Electrochemical impedance spectroscopy (EIS) spectra were collected in the

https://doi.org/10.1021/acsaem.3c03091
ACS Appl. Energy Mater. 2024, 7, 2329−2337

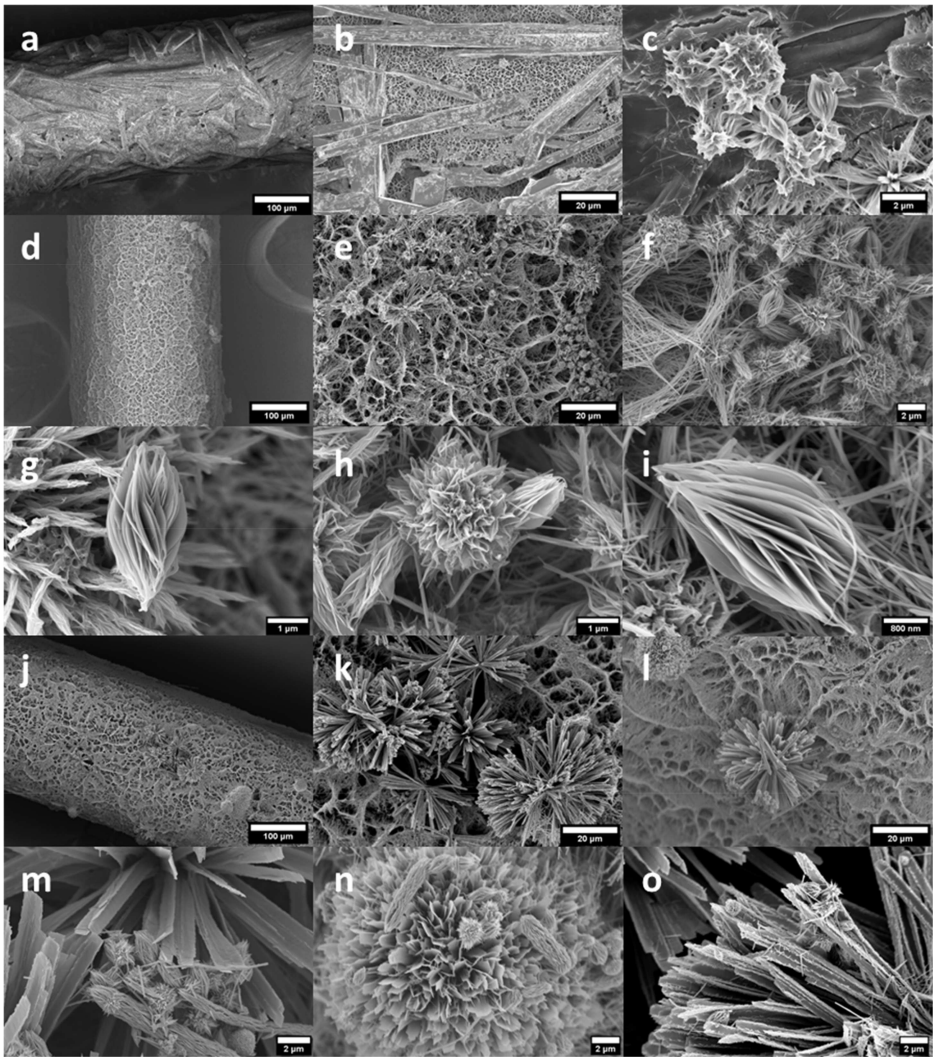

Figure 2. SEM images for Ti wires treated with NaOH for 4 h (a–c), 12 h (d–i), and 24 h (j–o) with different magnifications.

frequency range between 0.1 and 100 Hz, with the applied bias voltage the same as the open-circuit voltage of the cells.

RESULTS AND DISCUSSION

Device Structure. During cell fabrication, a Pt-wire counter electrode (CE) is aligned parallel to the working electrode (WE) instead of wrapping around it (Figure 1). This device geometry is adopted to minimize the contact between the WE and Pt CE to avoid short circuiting due to direct contact between Ti metal underneath the TiO_2 layer and Pt metal in the CE. In addition, this cell design uses less Pt wire, which could lower the expense in cell fabrication. Note that Pt-coated carbon nanotube yarns are not chosen for this study because this type of CE needs additional preparation steps, and its wire-to-wire and batch-to-batch differences forbid it to serve as a good standard to compare the WE prepared under different conditions. Finally, Pt wires can facilitate ease of good connection and photovoltaic measurement.

Morphology Characterization. Figure 2 shows that Ti wires reacted with a 2.5 M NaOH solution in an autoclave at 220 °C for three different time lengths: 4, 12, and 24 h. Figure 2a is the overview for a large area for the treated Ti wire. After reacting with a NaOH solution for 4 h, the surface of the wire becomes uneven. Higher magnification images of this sample are shown in Figure 2b,c. Figure 2b indicates that even with this short period of reaction time, TiO_2 NWs began to form on the surface of the Ti wire, which are the light-colored network. However, there is still a large portion of bare Ti metal. Figure 2c reveals two flowerlike hierarchical TiO_2 structures: one is budlike, with flat semioval-shaped platelets vertically circling the axis of the bud; the other is similar to a bloomed flower, where pedals are twisted platelets. At this stage of the reaction, both structures are not yet well developed.

Figure 2d is the overview for a large area for the Ti wire with NaOH treatment for 12 h. The surface is now rough and covered with a network, showing growth of the TiO_2 NW layer on top of Ti. This can be proven in Figure 2e,f, which clearly shows the formed TiO_2 NWs. Besides, both parts e and f of Figure 2 show budlike and bloomed-flowerlike hierarchical structures. Compared to those shown in Figure 2c, after 12 h of reaction, both structures are better defined and have finer details, i.e., thinner platelets/pedals in a larger number. Details of these two hierarchical structures from the 12 h sample are shown with high magnification in Figure 2g–i. Interestingly, wires can be observed on the tips of these platelets/pedals in both structures, especially the budlike ones (Figure 2g,i).

Parts j–o of Figure 2 are images of Ti wires treated with a NaOH solution for 24 h. In Figure 2j, large TiO_2 microflowers

https://doi.org/10.1021/acsaem.3c03091
ACS Appl. Energy Mater. 2024, 7, 2329–2337

(diameter ~20 μm) can be directly observed on the surface of Ti wires, even with the lowest magnification. Compared to the microflowers shown in Shao et al.'s work,[35] more different types of hierarchical structures are obtained. The large microflower shown in Figure 2n resembles those in Shao et al.'s work,[35] while another kind (Figure 2k–m,o) has a different arrangement of nanobelts. On top of these microflowers, smaller hierarchical structures can also be seen (Figure 2m–o): budlike and bloomed-flowerlike hierarchical structures and another type with an appearance similar to that of a golden torch cactus.

SEM images of Ti wires with hydrothermal treatment for 8, 16, and 20 h are shown in Figure S1. Although budlike and bloomed-flowerlike hierarchical structures are shown in 4-h treatment samples, 8-h images are predominantly NW arrays. This can be explained by the fact that, in the early stage of hydrothermal reaction, NW growth is the major procedure; meanwhile, there may be a batch-to-batch difference. Nevertheless, the general trend is that, with longer treatment time, there are more hierarchical structures on top of NW arrays.

Note that large microflower structures only appear with the longest treatment time (24 h) in this work, while those small hierarchical structures can be observed on wires with almost all different treatment times. In addition, these structures are always at the most outside layer of the wire. Furthermore, the SEM images reflect the connection between these hierarchical structures and NWs. In Figure 2g,i, wires can be seen on top of the platelets/pedals in these structures; wire/needlelike structures are also observed at the edges of nanobelts, which form the large microflowers (Figure 2o).

On the basis of the above experimental results and Shao et al.'s work,[35] we propose the following explanation for the formation of these different kinds of TiO_2 hierarchical structures. $Na_2Ti_2O_5{\cdot}H_2O$ formed during a NaOH hydrothermal reaction on a Ti wire dissolves in the solution and recrystallizes, which acts as the nuclei for NW/nanobelt growth in all directions. These nanostructures then arrange in different patterns to form different hierarchical structures.

Note that, although this work shares some similarities with the study done by Shao et al.[35] (reacting Ti metal with a NaOH solution), there are still differences: Ti wires are used in our experiment instead of Ti foil, which may lead to different masses of Ti used; the concentration of NaOH is lower in this work, so the ratio of Ti metal/NaOH differs. This eventually resulted in very different morphologies after hydrothermal treatment: Shao et al.[35] reported a complete layer of TiO_2 microflowers with uniform structure on top of TiO_2 NW arrays, while in this work, we obtained various different hierarchical structures.

Figures 2 and S1 were all taken after calcination at 550 °C. SEM images of Ti wires undergoing a 12-h hydrothermal reaction before and after HCl treatment without calcination at 550 °C are shown in Figure S2. Compared to Figure 2d–f, it is clear that the NWs and budlike and bloomed-flowerlike hierarchical structures are formed in the hydrothermal reaction. The following treatments do not change the morphology of the TiO_2 structures on top of the Ti wire.

Crystal Structure. Figure 3 shows the X-ray diffraction (XRD) patterns of Ti wires reacted with 2.5 M NaOH for different time periods. The sample with a 4-h reaction time shows patterns that can be attributed to α-Ti (ICDD PDF 00-001-1198). The peaks that appear at 2θ = 35.3°, 38.4°, 40.4°, 53.2°, 63.2°, 70.8°, 74.0°, and 76.1° correspond to α-Ti (100), (002), (101), (102), (110), (103), (200), and (112) crystal planes, respectively. This is also in accordance with SEM images (Figure 2a–c). Although TiO_2 NWs and hierarchical structures begin to grow on the surface of the Ti wire, they do not occupy all of the surface area, and the thickness of this incomplete TiO_2 NW/hierarchical structure layer is very small due to the short treatment time. Therefore, the dominant XRD signal is from Ti metal.

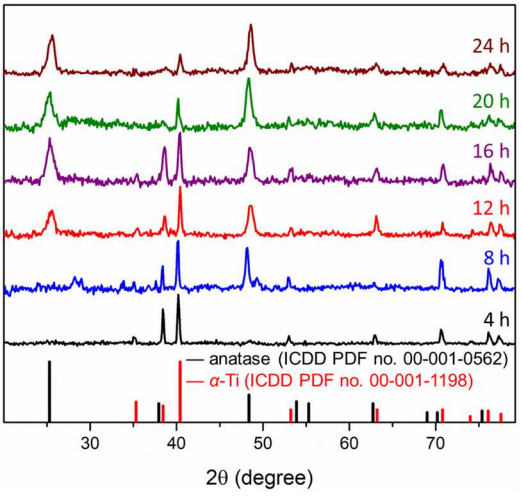

Figure 3. XRD patterns of Ti wires treated with NaOH with different time lengths (4, 8, 12, 16, 20, and 24 h). XRD peak positions for anatase and α-Ti are also present forcomparison. All spectra are normalized with respect to the most intense peak.

Starting from the 8-h treatment time, the peak at $2\theta \cong 48.4°$, which corresponds to the crystal plane of anatase TiO_2 (200), begins to appear. In addition, the peak at $2\theta \cong 25.3°$ increases in relative intensity, which is the XRD signal from the anatase TiO_2 (100) crystal plane. At the same time, XRD signals due to Ti metal at $2\theta \cong 38.4°$ and 40.4° have decreasing relative intensity. It can be understood that, with increasing reaction time, a TiO_2 layer covers the whole surface of the Ti wire (Figure 2d). In addition, a longer reaction time results in a thicker TiO_2 layer. Therefore, the XRD signal changes from bare Ti to anatase TiO_2, which agrees with the work done by Shao et al.[25] The XRD data also indicate that, although the morphologies of these different types of flowerlike hierarchical structures look very different from those of TiO_2 NWs, they still have the same crystal structure.

Photovoltaic Characterizations. A photovoltaic performance study for different cell lengths with photoanodes treated with NaOH for different time periods is summarized in Figure 4. A length-dependent study for 12-h and 24-h hydrothermal reaction time (Figure 4a,b) shows that the short-circuit current (J_{SC}) fluctuates with different cell lengths and the open-circuit voltage (V_{OC}) decreases with shorter cell length. The general trend for V_{OC} change is also observed in other samples (Figure 4d). However, J_{SC} dependence on the length for other samples differs from the trend observed in the 12-h and 24-h samples (Figure 4c). For example, the 4-h sample (Figure 4c, black line) has J_{SC} slight increasing with longer cell lengths, while the 16-h and 20-h samples show a general increasing trend of J_{SC} with decreasing cell length. The filling factor (FF) of most cells ranges from 0.632 to 0.705 and shows no dependence on the cell length, except for the 4-h sample 1.0, 1.5, and 2.0 cm cell lengths. The incomplete TiO_2 layer on the Ti wire for the 4-h

https://doi.org/10.1021/acsaem.3c03091
ACS Appl. Energy Mater. 2024, 7, 2329–2337

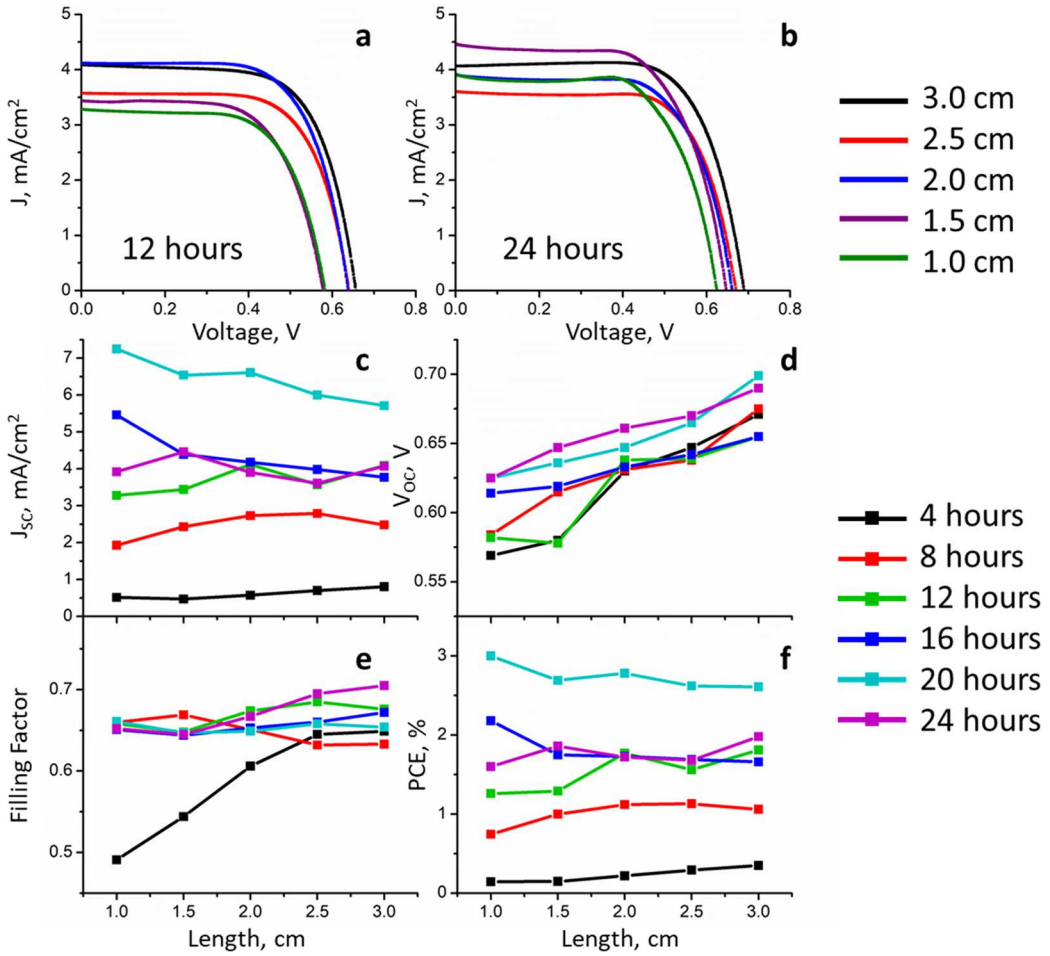

Figure 4. Length-dependent study for cells with photoanodes treated with NaOH for different time periods: (a and b) $J-V$ curves for the 12-h and 24-h samples at different lengths (3.0, 2.5, 2.0, 1.5, and 1.0 cm), respectively; (c–f) length dependence of J_{SC}, V_{OC}, FF, and PCE, respectively, obtained for photoanodes treated with NaOH for different time periods. The actual values of PCE shown in part f are listed in Table S4.

sample shown in SEM images could explain the poor photovoltaic performance of this sample.

From the comparison in Figure 4c–f, although V_{OC} shows a general increasing trend with longer cell length for all samples, the trend in the power conversion efficiency (PCE) mostly resembles the trend in J_{SC}, which means J_{SC} plays the dominant role in determining the PCE of these cells. The best cell performance observed in this study is the 1 cm cell length with NaOH treatment for 20 h. Among all samples, this cell has the highest J_{SC} (7.25 mA/cm^2) and PCE (3.00%). In the length-dependent study, the 12-h, 16-h, and 24-h samples show similar cell performance parameters, which shows that an incomplete layer of microflowers is not sufficient to enhance light absorption;[35] therefore, the 24-h sample does not show an increase in the cell performance compared to the 20-h sample, which does not have microflowers.

The change of J_{SC} at various conditions can be attributed to two reasons: the dye loading amount and the electron diffusion length. The first factor, the dye loading amount, is dependent on the structure and thickness of the TiO_2 layer. In different works,[35,45,46] this value is usually reported in the range between 10^{-8} and 10^{-7} μmol/cm^2. In the work done by Shao et al.,[35] the Brunauer–Emmett–Teller surface area of TiO_2 was measured to be about 37 m^2/g, and the pores' volume was estimated to be 0.34 cm^3/g. Therefore, increasing the TiO_2 thickness causes an increase in the adsorption sites of the dye molecule. In our experiment, based on the SEM images, a longer NaOH treatment time resulted in thicker TiO_2 layers, which caused a higher loading amount of N719 dye, and eventually led to an increase in J_{SC} in cells that reacted with NaOH for a longer time. The other factor that can explain the trend in J_{SC} of cells with longer NaOH treatment time is the electron diffusion length. Zhu et al.[20] showed that, in TiO_2 nanorods, the average distance for an injected electron to travel was about 11.4 μm before recombination. If the TiO_2 layer on the photoanode is thicker than this length, the injected electron will be lost due to charge recombination.[25] Therefore, it is reasonable to assume that when the NaOH reaction time is too long, the resulting TiO_2 layer is too thick for electron diffusion, and the increase in the dye adsorption amount cannot compensate for it, so J_{SC} and PCE for the cells are no longer monotonic functions of the NaOH treatment time if the hydrothermal process is too long.

The incident photon-to-current efficiency (IPCE) results of a TiO_2 + N719 dye combination are well studied, for example, the work done by Shao et al.[25] and An et al.[47] Usually, the plot has a very broad peak, which starts from the 300–400 nm region and tails to wavelengths higher than 700 nm. At the peak of the spectrum, the IPCE % can range from 20% to over 90%, depending on the TiO_2 structure and surface treatment method.[25,47] Because J_{SC} of a device can be obtained via integration of the IPCE curve,[48] the factors that affect J_{SC} will

https://doi.org/10.1021/acsaem.3c03091
ACS Appl. Energy Mater. 2024, 7, 2329–2337

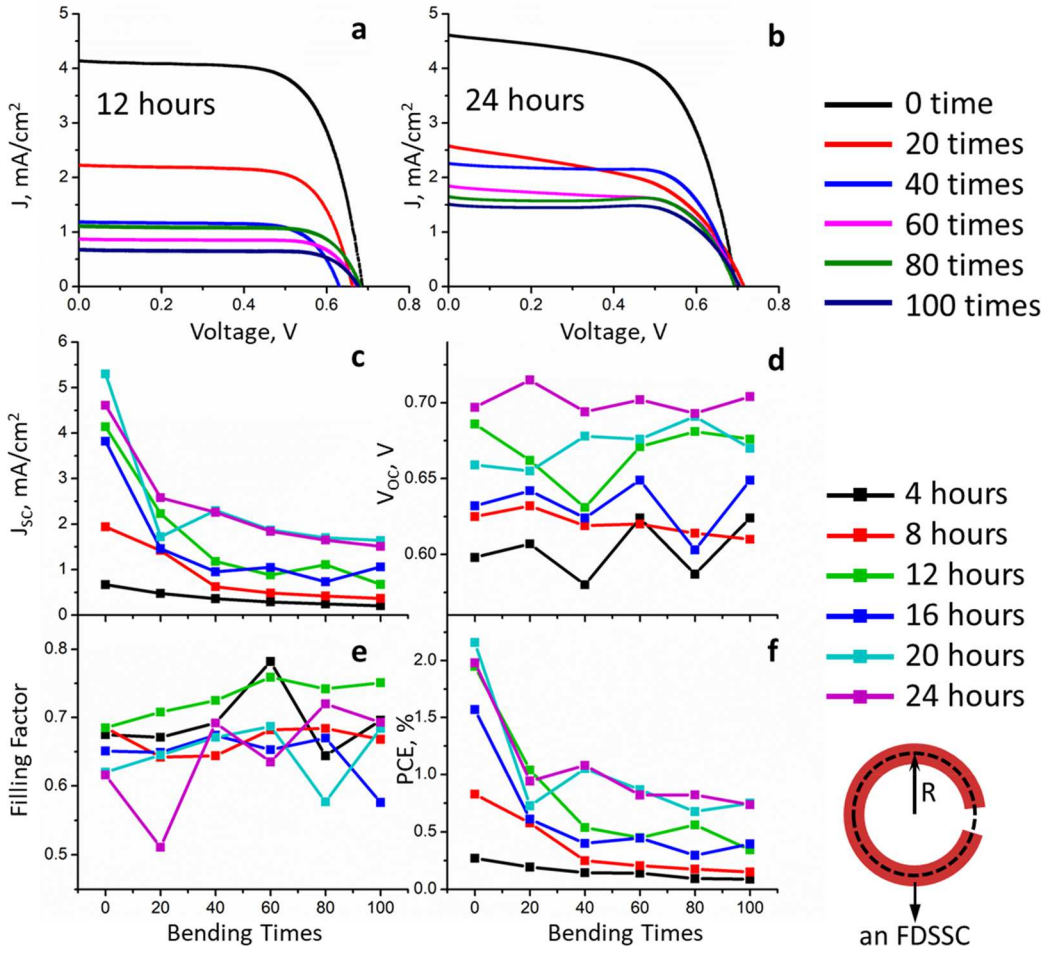

Figure 5. Bending times study for cells with photoanodes treated with NaOH for different time periods: (a and b) $J-V$ curves for the 12-h and 24-h samples at different bending times (0, 20, 40, 60, 80, and 100), respectively; (c–f) bending-time dependence of J_{SC}, V_{OC}, FF, and PCE, respectively, obtained for photoanodes treated with NaOH for different time periods. The cells are all bent with $R \sim 0.5$ cm. The actual values of the PCE shown in part f are listed in Table S4.

have a similar effect on the IPCE, especially the dye adsorption amount and charge collection efficiency.[48]

One interesting thing is that V_{OC} is generally increasing slightly with longer cell lengths. Generally, higher V_{OC} can be attributed to lower electron recombination.[49] It is possible that when the cell is shorter, injected charges have more limited space to move; thus, the recombination increases, leading to lower V_{OC} values.

The cell properties with different bending times of cells with varying NaOH treatment times are shown in Figure 5. In the bending study, only one bending degree is chosen, which corresponds to a bending radius (R) of ~0.5 cm. There are two reasons to choose this bending degree: first, cells fabricated in this study are relatively short (3.0 cm), and considering the certain rigidity of the Ti wire base, this bending degree could ensure that the bending evenly distributed over the whole cell; second, although most studies focus on the bending extent to which cells could maintain their performance, we want to investigate the situation when cells are under extreme bending condition; i.e., the cells are bent many times with extremely small bending radius, and the cell experiences a significant performance decrease. The cells used for the bending times study are different from those of the length-dependent study (the photoanodes are from the same batch); therefore, some fluctuations in the cell performance are expected.

Figure 5 reveals that, during the first 20 bending times, most cells experience a dramatic drop in J_{SC} and PCE. For example, the 12-h sample (Figure 5a) has a decrease in J_{SC} from 4.14 to 2.23 mA/cm^2 and in PCE from 1.95% to 1.04% (both decrease by ~46%); the 24-h sample (Figure 5b) has a 44% decrease in J_{SC} and a 52% decrease PCE; the largest decrease appears in the 20-h sample, and the corresponding decrease percentage is ~67%. This could be understood that, for the first 20 times of extreme bending, TiO_2-nanostructured layers (NWs + hierarchical structures) on top of Ti wires are damaged to a large extent, causing a dramatic decrease in the cell performance. However, additional bending times do not decrease the cell performance as large as the first 20 times, and some samples have fluctuation in their cell parameters, such as the 20-h and 24-h samples: both J_{SC} and PCE increase after 40 bending times compared to the data after 20 bending times.

EIS was adopted to investigate the reason for the decreasing cell performance. The Nyquist plots for cells treated with NaOH for 24 h were collected after three different bending times, as shown in Figure 6. According to the literature,[50−52] the offset between the plot and the vertical axis, the smaller semicircle at high frequencies, and the larger semicircle at low frequencies can provide information about the internal resistance (R_1), CE/electrolyte interface charge-transfer

https://doi.org/10.1021/acsaem.3c03091
ACS Appl. Energy Mater. 2024, 7, 2329−2337

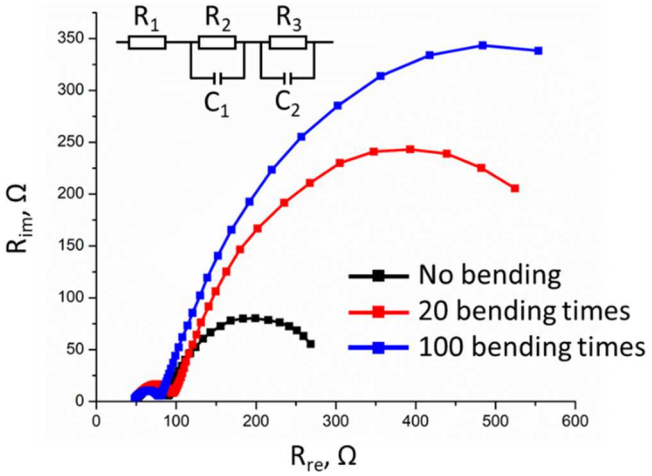

Figure 6. EIS spectra for DSSCs with 24-h NaOH treatment at various bending times. The inserted image is the equivalent circuit used for fitting.

resistance (R_2), and a combination of TiO_2/N719/electrolyte interface charge-transfer resistances (R_3), respectively. In Figure 6, the most abrupt change happens on the semicircle at low frequency, which dramatically increases with increasing bending times. Spectra fitting yields R_3 value increases at different bending times: 178 Ω without bending, 495 Ω after bending 20 times, and 673 Ω after bending 100 times. This demonstrates that the bending largely damaged the interface of the TiO_2/N719/electrolyte, which blocks charge transfer, and resulted in an increase of the R_3 value as well as a decrease of J_{SC}.

The bending times study also shows that V_{OC} and FF are relatively independent from the bending times. Theoretically, V_{OC} of a DSSC is defined as the difference in potential between the electrolyte redox level and the quasi-Fermi energy level of TiO_2 under illumination.[53] Although the EIS data show that bending largely affects the charge-transfer resistance at the interface of the TiO_2/dye/electrolyte, the electrolyte redox potential and the quasi-Fermi energy level of TiO_2 under illumination are unaffected, resulting in a stable V_{OC} value after various bending times. From Figure 5d, the 24-h sample has on average the largest V_{OC} of all samples after different bending times, while the 12-h sample holds a V_{OC} variation range similar to that of the 20-h sample and higher than those of the 4-h, 8-h, and 16-h sample. In addition, the 12-h sample for the bending study shows a small change in FF and has on average larger values at different bending conditions than other samples. Because the 12-h sample has better V_{OC} and FF, although its J_{SC} is similar to that of the 16-h sample during the bending study, its PCE has a larger value. Note that the cell performances of the 12-h, 16-h, 20-h, and 24-h samples after 100 bending times are still better than those for the 4-h sample without any bending. Thus, the cells with photoanodes treated with NaOH for 12 h or longer time will experience a larger performance drop in the beginning of extreme bending conditions, while they can still maintain a certain level of performance toward long run. Also, a better cell performance could be possibly achieved with increasing bending radius (less extreme bending conditions), which could make the devices suitable for various different applications where flexibility is required.

CONCLUSION

In summary, the fabrication of a photoanode with TiO_2 hierarchical structure on top of TiO_2 NWs for FDSSCs has been reported. A hydrothermal reaction with NaOH followed by a HCl treatment and annealing method has been used to obtain the desired TiO_2 morphology. A relative comparison of the performance obtained from devices based on photoanodes reacted with NaOH with different time lengths has been performed via length-dependent and extreme bending tests. We conclude that these different hierarchical TiO_2 structures are formed due to different arrangements of nanostructures grown on dissolved and recrystallized $Na_2Ti_2O_5{\cdot}H_2O$. In photovoltaic studies, these hierarchical structures could help to maintain the cell performance by maintaining relatively high and stable V_{OC} and FF.

ASSOCIATED CONTENT

Supporting Information

The Supporting Information is available free of charge at https://pubs.acs.org/doi/10.1021/acsaem.3c03091.

SEM images for Ti wires treated with NaOH for 8, 16, and 20 h, SEM images for Ti wires without calcination, and tables of PCE values for length-dependent and bending times studies (PDF)

AUTHOR INFORMATION

Corresponding Author

Mohammed Jasim Uddin − *Photonic and Energy Research Laboratory, The University of Texas, Rio Grande Valley, Edinburg, Texas 78539, United States;* orcid.org/0000-0002-7935-7269; Email: mohammed.uddin@utrgv.edu

Authors

Chen Lin − *Photonic and Energy Research Laboratory, The University of Texas, Rio Grande Valley, Edinburg, Texas 78539, United States;* orcid.org/0000-0003-0036-9994

Brishty Deb Choudhury − *Photonic and Energy Research Laboratory, The University of Texas, Rio Grande Valley, Edinburg, Texas 78539, United States*

Rigobert Ybarra − *Photonic and Energy Research Laboratory, The University of Texas, Rio Grande Valley, Edinburg, Texas 78539, United States*

Sk Md Ali Zaker Shawon − *Photonic and Energy Research Laboratory, The University of Texas, Rio Grande Valley, Edinburg, Texas 78539, United States*

Haimanti Majumder − *Photonic and Energy Research Laboratory, The University of Texas, Rio Grande Valley, Edinburg, Texas 78539, United States*

Javier Soliz-Martinez − *Department of Mechanical Engineering, The University of Texas, Rio Grande Valley, Edinburg, Texas 78539, United States*

Nicolas Dimakis − *Department of Physics and Astronomy, The University of Texas, Rio Grande Valley, Edinburg, Texas 78539, United States;* orcid.org/0000-0003-2478-237X

Karen Lozano − *Department of Mechanical Engineering, The University of Texas, Rio Grande Valley, Edinburg, Texas 78539, United States;* orcid.org/0000-0002-6676-8632

Complete contact information is available at: https://pubs.acs.org/10.1021/acsaem.3c03091

Author Contributions

†B.D.C. and R.Y. contributed equally.

Notes

The authors declare no competing financial interest.

■ ACKNOWLEDGMENTS

B.D.C. gratefully acknowledges the Presidential Graduate Research Assistantship, Welch Foundation (Grant BX0048), and National Science Foundation (Award 2122178), UTRGV−UMN Partnership to Strengthen the PREM Pathway. R.Y. acknowledges support from the Department of Energy (Award DE-NA0004004), Integrated Additive Manufacturing Establishing Minority Pathways: Opportunities for Workforce-development in Energy Research and Education (IAM-EMPOWERED).

■ REFERENCES

(1) Chen, X.; Mao, S. S. Titanium Dioxide Nanomaterials: Synthesis, Properties, Modifications, and Applications. *Chem. Rev.* **2007**, *107* (7), 2891−2959.
(2) Wang, X. D.; Li, Z. D.; Shi, J.; Yu, Y. H. One-Dimensional Titanium Dioxide Nanomaterials: Nanowires, Nanorods, and Nanobelts. *Chem. Rev.* **2014**, *114* (19), 9346−9384.
(3) Salvador, A.; Pascual-Marti, M. C.; Adell, J. R.; Requeni, A.; March, J. G. Analytical Methodologies for Atomic Spectrometric Determination of Metallic Oxides in UV Sunscreen Creams. *J. Pharm. Biomed. Anal.* **2000**, *22* (2), 301−306.
(4) Zallen, R.; Moret, M. P. The Optical Absorption Edge of Brookite TiO_2. *Solid State Commun.* **2006**, *137* (3), 154−157.
(5) Braun, J. H.; Baidins, A.; Marganski, R. E. TiO_2 Pigment Technology - a Review. *Prog. Org. Coat.* **1992**, *20* (2), 105−138.
(6) Yuan, S. A.; Chen, W. H.; Hu, S. S. Fabrication of Tio2 Nanoparticles/Surfactant Polymer Complex Film on Glassy Carbon Electrode and Its Application to Sensing Trace Dopamine. *Mater. Sci. Eng. C-Biomimetic Supramol. Syst.* **2005**, *25* (4), 479−485.
(7) Jiu, J. T.; Isoda, S.; Wang, F. M.; Adachi, M. Dye-Sensitized Solar Cells Based on a Single-Crystalline TiO_2 Nanorod Film. *J. Phys. Chem. B* **2006**, *110* (5), 2087−2092.
(8) Liu, B.; Aydil, E. S. Growth of Oriented Single-Crystalline Rutile TiO_2 Nanorods on Transparent Conducting Substrates for Dye-Sensitized Solar Cells. *J. Am. Chem. Soc.* **2009**, *131* (11), 3985−3990.
(9) Bach, U.; Lupo, D.; Comte, P.; Moser, J. E.; Weissortel, F.; Salbeck, J.; Spreitzer, H.; Gratzel, M. Solid-State Dye-Sensitized Mesoporous TiO_2 Solar Cells with High Photon-to-Electron Conversion Efficiencies. *Nature* **1998**, *395* (6702), 583−585.
(10) Law, M.; Greene, L. E.; Radenovic, A.; Kuykendall, T.; Liphardt, J.; Yang, P. D. ZnO-Al_2O_3 and ZnO-TiO_2 Core-Shell Nanowire Dye-Sensitized Solar Cells. *J. Phys. Chem. B* **2006**, *110* (45), 22652−22663.
(11) Greene, L. E.; Law, M.; Yuhas, B. D.; Yang, P. D. ZnO- TiO_2 Core-Shell Nanorod/P3HT Solar Cells. *J. Phys. Chem. C* **2007**, *111* (50), 18451−18456.
(12) Liu, J. W.; Kuo, Y. T.; Klabunde, K. J.; Rochford, C.; Wu, J.; Li, J. Novel Dye-Sensitized Solar Cell Architecture Using TiO_2-Coated Vertically Aligned Carbon Nanofiber Arrays. *ACS Appl. Mater. Interfaces* **2009**, *1* (8), 1645−1649.
(13) Burschka, J.; Pellet, N.; Moon, S. J.; Humphry-Baker, R.; Gao, P.; Nazeeruddin, M. K.; Gratzel, M. Sequential Deposition as a Route to High-Performance Perovskite-Sensitized Solar Cells. *Nature* **2013**, *499* (7458), 316−319.
(14) Ip, A. H.; Thon, S. M.; Hoogland, S.; Voznyy, O.; Zhitomirsky, D.; Debnath, R.; Levina, L.; Rollny, L. R.; Carey, G. H.; Fischer, A.; Kemp, K. W.; Kramer, I. J.; Ning, Z. J.; Labelle, A. J.; Chou, K. W.; Amassian, A.; Sargent, E. H. Hybrid Passivated Colloidal Quantum Dot Solids. *Nat. Nanotechnol.* **2012**, *7* (9), 577−582.
(15) Gunes, S.; Neugebauer, H.; Sariciftci, N. S. Conjugated Polymer-Based Organic Solar Cells. *Chem. Rev.* **2007**, *107* (4), 1324−1338.
(16) Kim, J. Y.; Kim, S. H.; Lee, H. H.; Lee, K.; Ma, W. L.; Gong, X.; Heeger, A. J. New Architecture for High-Efficiency Polymer Photovoltaic Cells Using Solution-Based Titanium Oxide as an Optical Spacer. *Adv. Mater.* **2006**, *18* (5), 572−576.
(17) Roduner, E. Size Matters: Why Nanomaterials Are Different. *Chem. Soc. Rev.* **2006**, *35* (7), 583−592.
(18) Lopez-Luke, T.; Wolcott, A.; Xu, L. P.; Chen, S. W.; Wen, Z. H.; Li, J. H.; De La Rosa, E.; Zhang, J. Z. Nitrogen-Doped and Cdse Quantum-Dot-Sensitized Nanocrystalline TiO_2 Films for Solar Energy Conversion Applications. *J. Phys. Chem. C* **2008**, *112* (4), 1282−1292.
(19) Law, M.; Greene, L. E.; Johnson, J. C.; Saykally, R.; Yang, P. D. Nanowire Dye-Sensitized Solar Cells. *Nat. Mater.* **2005**, *4* (6), 455−459.
(20) Zhu, K.; Neale, N. R.; Miedaner, A.; Frank, A. J. Enhanced Charge-Collection Efficiencies and Light Scattering in Dye-Sensitized Solar Cells Using Oriented TiO_2 Nanotubes Arrays. *Nano Lett.* **2007**, *7* (1), 69−74.
(21) Chen, D.; Zhang, H.; Hu, S.; Li, J. H. Preparation and Enhanced Photoelectrochemical Performance of Coupled Bicomponent ZnO-TiO_2 Nanocomposites. *J. Phys. Chem. C* **2008**, *112* (1), 117−122.
(22) Kang, S. H.; Choi, S. H.; Kang, M. S.; Kim, J. Y.; Kim, H. S.; Hyeon, T.; Sung, Y. E. Nanorod-Based Dye-Sensitized Solar Cells with Improved Charge Collection Efficiency. *Adv. Mater.* **2008**, *20* (1), 54−58.
(23) Yang, W. G.; Wan, F. R.; Wang, Y. L.; Jiang, C. H. Achievement of 6.03% Conversion Efficiency of Dye-Sensitized Solar Cells with Single-Crystalline Rutile TiO_2 Nanorod Photoanode. *Appl. Phys. Lett.* **2009**, *95* (13), No. 133121.
(24) Fujihara, K.; Kumar, A.; Jose, R.; Ramakrishna, S.; Uchida, S. Spray Deposition of Electrospun TiO_2 Nanorods for Dye-Sensitized Solar Cell. *Nanotechnology* **2007**, *18* (36), No. 365709.
(25) Shao, F.; Sun, J.; Gao, L. A.; Yang, S. W.; Luo, J. Q. Growth of Various TiO_2 Nanostructures for Dye-Sensitized Solar Cells. *J. Phys. Chem. C* **2011**, *115* (5), 1819−1823.
(26) Wang, R.; Cai, X.; Shen, F. L. Preparation of TiO_2 Hollow Microspheres by a Novel Vesicle Template Method and Their Enhanced Photocatalytic Properties. *Ceram. Int.* **2013**, *39* (8), 9465−9470.
(27) Li, F. B.; Li, X. Z.; Hou, M. F.; Cheah, K. W.; Choy, W. C. H. Enhanced Photocatalytic Activity of Ce^{3+}-TiO_2 for 2-Mercaptobenzothiazole Degradation in Aqueous Suspension for Odour Control. *Appl. Catal. A-Gen.* **2005**, *285* (1−2), 181−189.
(28) Yu, J. G.; Yu, J. C.; Ho, W. K.; Leung, M. K. P.; Cheng, B.; Zhang, G. K.; Zhao, X. J. Effects of Alcohol Content and Calcination Temperature on the Textural Properties of Bimodally Mesoporous Titania. *Appl. Catal. A-Gen.* **2003**, *255* (2), 309−320.
(29) Yun, J.; Jin, D.; Lee, Y. S.; Kim, H. I. Photocatalytic Treatment of Acidic Waste Water by Electrospun Composite Nanofibers of pH-Sensitive Hydrogel and TiO_2. *Mater. Lett.* **2010**, *64* (22), 2431−2434.
(30) Chan, C. K.; Peng, H. L.; Liu, G.; McIlwrath, K.; Zhang, X. F.; Huggins, R. A.; Cui, Y. High-Performance Lithium Battery Anodes Using Silicon Nanowires. *Nat. Nanotechnol.* **2008**, *3* (1), 31−35.
(31) Boettcher, S. W.; Spurgeon, J. M.; Putnam, M. C.; Warren, E. L.; Turner-Evans, D. B.; Kelzenberg, M. D.; Maiolo, J. R.; Atwater, H. A.; Lewis, N. S. Energy-Conversion Properties of Vapor-Liquid-Solid-Grown Silicon Wire-Array Photocathodes. *Science* **2010**, *327* (5962), 185−187.
(32) Wang, Y. Z.; Hong, X.; Wang, G. Z.; Wang, X. P. Fabrication and Photocatalysis of TiO_2 Flower-Like Nanostructures. *Chin. J. Chem. Phys.* **2006**, *19* (6), 559−562.
(33) Hyam, R. S.; Bhosale, R. K.; Lee, W.; Han, S. H.; Hannoyer, B.; Ogale, S. B. Room Temperature Synthesis of Rutile TiO_2 Hierarchical Nanoneedle Flower Morphology for Dye Sensitized Solar Cell. *J. Nanosci. Nanotechnol.* **2010**, *10* (9), 5894−5898.
(34) Xiang, Q. J.; Yu, J. G. Photocatalytic Activity of Hierarchical Flower-Like TiO_2 Superstructures with Dominant {001} Facets. *Chin. J. Catal.* **2011**, *32* (4), 525−531.

https://doi.org/10.1021/acsaem.3c03091
ACS Appl. Energy Mater. 2024, 7, 2329−2337

(35) Shao, F.; Sun, J.; Gao, L.; Yang, S. W.; Luo, J. Q. Template-Free Synthesis of Hierarchical TiO_2 Structures and Their Application in Dye-Sensitized Solar Cells. *ACS Appl. Mater. Interfaces* **2011**, *3* (6), 2148−2153.
(36) Xu, N. X.; Hu, L.; Zhang, Q. L.; Xiao, X. R.; Yang, H.; Yu, E. J. Significantly Enhanced Dielectric Performance of Poly(Vinylidene Fluoride-Co-Hexafluoropylene)-Based Composites Filled with Hierarchical Flower-Like TiO_2 Particles. *ACS Appl. Mater. Interfaces* **2015**, *7* (49), 27373−27381.
(37) Zhao, L.; Zhong, C.; Wang, Y. L.; Wang, S. M.; Dong, B. H.; Wan, L. Ag Nanoparticle-Decorated 3D Flower-Like TiO_2 Hierarchical Microstructures Composed of Ultrathin Nanosheets and Enhanced Photoelectrical Conversion Properties in Dye-Sensitized Solar Cells. *J. Power Sources* **2015**, *292*, 49−57.
(38) Li, H. L.; Li, T. D.; Liu, H. X.; Huang, B. B.; Zhang, Q. Hierarchical Flower-Like Nanostructures of Anatase TiO_2 Nanosheets Dominated by {001} Facets. *J. Alloy. Compd.* **2016**, *657*, 1−7.
(39) Que, Y. P.; Weng, J.; Hu, L. H.; Wu, J. H.; Dai, S. Y. High Open Voltage and Superior Light-Harvesting Dye-Sensitized Solar Cells Fabricated by Flower-Like Hierarchical TiO_2 Composed with Highly Crystalline Nanosheets. *J. Power Sources* **2016**, *307*, 138−145.
(40) Zong, L. Y.; Zhang, G. D.; Zhao, J. H.; Dong, F.; Zhang, J. Y.; Tang, Z. C. Morphology-Controlled Synthesis of 3d Flower-Like TiO_2 and the Superior Performance for Selective Catalytic Reduction of NO_x with NH_3. *Chem. Eng. J.* **2018**, *343*, 500−511.
(41) Liu, H. X.; Zhang, L. N.; Li, T. D. A Study of Controllable Synthesis and Formation Mechanism on Flower-Like TiO_2 with Spherical Structure. *Crystals* **2018**, *8* (12), 466.
(42) Zhang, J. X.; Wang, Z. P.; Li, X. L.; Yang, J.; Song, C. H.; Li, Y. P.; Cheng, J. L.; Guan, Q.; Wang, B. Flexible Platinum-Free Fiber-Shaped Dye Sensitized Solar Cell with 10.28% Efficiency. *ACS Appl. Energy Mater.* **2019**, *2* (4), 2870−2877.
(43) Liu, G. C.; Wang, H.; Wang, M. X.; Liu, W. B.; Anugrah Ardhi, R. E.; Zou, D. C.; Lee, J. K. Study on a Stretchable, Fiber-Shaped, and TiO_2 Nanowire Array-Based Dye-Sensitized Solar Cell with Electrochemical Impedance Spectroscopy Method. *Electrochim. Acta* **2018**, *267*, 34−40.
(44) Chu, L.; Li, L. Y.; Su, J.; Tu, F. F.; Liu, N. S.; Gao, Y. H. A General Method for Preparing Anatase TiO_2 Treelike-Nanoarrays on Various Metal Wires for Fiber Dye-Sensitized Solar Cells. *Sci. Rep.* **2014**, *4*, 4420.
(45) Lee, C. R.; Kim, H. S.; Jang, I. H.; Im, J. H.; Park, N. G. Pseudo First-Order Adsorption Kinetics of N719 Dye on TiO_2 Surface. *ACS Appl. Mater. Interfaces* **2011**, *3* (6), 1953−1957.
(46) Wang, Z. S.; Kawauchi, H.; Kashima, T.; Arakawa, H. Significant Influence of TiO_2 Photoelectrode Morphology on the Energy Conversion Efficiency of N719 Dye-Sensitized Solar Cell. *Coord. Chem. Rev.* **2004**, *248*, 1381−1389.
(47) An, J.; Guo, W.; Ma, T. L. Enhanced Photoconversion Efficiency of All-Flexible Dye-Sensitized Solar Cells Based on a Ti Substrate with TiO_2 Nanoforest Underlayer. *Small* **2012**, *8* (22), 3427−3431.
(48) Devadiga, D.; Selvakumar, M.; Shetty, P.; Santosh, M. S. The Integration of Flexible Dye-Sensitized Solar Cells and Storage Devices Towards Wearable Self-Charging Power Systems: A Review. *Renew. Sust. Energy Rev.* **2022**, *159*, No. 112252.
(49) Mishra, A.; Fischer, M. K. R.; Bäuerle, P. Metal-Free Organic Dyes for Dye-Sensitized Solar Cells: From Structure: Property Relationships to Design Rules. *Angew. Chem.-Int. Ed.* **2009**, *48* (14), 2474−2499.
(50) Jose, R.; Thavasi, V.; Ramakrishna, S. Metal Oxides for Dye-Sensitized Solar Cells. *J. Am. Ceram. Soc.* **2009**, *92* (2), 289−301.
(51) Wang, Q.; Moser, J. E.; Grätzel, M. Electrochemical Impedance Spectroscopic Analysis of Dye-Sensitized Solar Cells. *J. Phys. Chem. B* **2005**, *109* (31), 14945−14953.
(52) Chen, J. K.; Li, K. X.; Luo, Y. H.; Guo, X. Z.; Li, D. M.; Deng, M. H.; Huang, S. Q.; Meng, Q. B. A Flexible Carbon Counter Electrode for Dye-Sensitized Solar Cells. *Carbon* **2009**, *47* (11), 2704−2708.
(53) Wang, H. X.; Liu, M. N.; Zhang, M.; Wang, P.; Miura, H.; Cheng, Y.; Bell, J. Kinetics of Electron Recombination of Dye-Sensitized Solar Cells Based on TiO_2 Nanorod Arrays Sensitized with Different Dyes. *Phys. Chem. Chem. Phys.* **2011**, *13* (38), 17359−17366.

https://doi.org/10.1021/acsaem.3c03091
ACS Appl. Energy Mater. 2024, 7, 2329−2337